ELSEVIER

Earth and Planetary Science Letters 5621 (2000) 201–213

EPSL

www.elsevier.com/locate/epsl

Fracturing in saturated rocks undergoing triaxial deformation using complex electrical conductivity measurements: experimental study

Paul W.J. Glover [a,*], Javier B. Gómez [b], P.G. Meredith [c]

[a] *Department of Geology and Petroleum Geology, University of Aberdeen, Aberdeen AB24 3UE, UK*
[b] *Departmento de Geología, Universidad de Zaragoza, Pza. San Francisco s/n, 50009 Zaragoza, Spain*
[c] *Department of Geological Sciences, University College London, Gower Street, London WC1E 6BT, UK*

Received 20 June 2000; accepted 28 August 2000

Abstract

Frequency dependent complex electrical conductivity measurements have been made on sandstones saturated with distilled water during triaxial deformation in both drained and undrained regimes. The resulting electrical and mechanical data show how the rock undergoes compaction, followed by dilatancy due to new crack formation, crack growth, interlinkage and failure as axial strain is increased. Electrical data are particularly good at indicating how early the formation of new cracks begins, showing that the quasi-linear portion of the stress–strain curve for triaxial deformation of saturated rocks does not represent truly elastic behaviour, but the combined effects of (i) crack closure perpendicular to the strain axis and (ii) the formation of tensile cracks parallel to the strain axis. A difference in the stress–strain behaviour between the drained and undrained samples was also observed, with the undrained samples developing a pronounced strain-softening phase before failure. The experimental data have also been used to derive the volumetric porosity, electrical porosity, cementation exponent and electrical tortuosity of the pore/crack network during deformation. The relative importance of crack closure and dilatation (a) during the progress of deformation and (b) between crack populations, controls these parameters and the electrical data over a wide range of frequencies. However, the frequency dependence of the micro-structural parameters and the electrical data was found to be not affected significantly by the hydrostatic pressurisation or the triaxial deformation. The development of large scale crack connectivity is observed to be confined to just prior to failure, and is controlled by the loss of cracks perpendicular to the axis of current flow and deformation.

Keywords: microcracks; fractures; electrical conductivity; triaxial tests; deformation; saturated materials

1. Introduction

The transport and mechanical properties of crustal rocks are inextricably linked. Damage induced by hydrostatic, uniaxial and triaxial loading changes the rock microstructure, and these changes affect the electrical, hydraulic and mechanical properties of the rock (e.g. [1–4]). Traditionally most effort has been given to understanding the effect of fluid flow through rocks (e.g.

* Corresponding author. Tel.: +44-1224-273453; Fax: +44-1224-272785; E-mail: p.glover@abdn.ac.uk

0012-821X/00/$ – see front matter
PII: S0012-821X(00)00267-3

[5–7]). However, electrical methods are growing in importance as a way of investigating the migration of fluids through crustal rocks [8–15]. This is because measurements of complex electrical conductivity as a function of frequency are extremely sensitive to changes in pore and crack volume, crack connectivity [16–17] and crack surface topography [11,18], making them very useful for obtaining information about the structure of the rock under a wide range of environmental conditions.

Examination of previous empirical determinations of fluid flow and electrical conductivity shows that although pore and crack networks vary tremendously in their geometry, rock transport properties seem to depend upon a small number of parameters [7]. Permeability during laminar flow seems to be controlled by a single length scale, porosity and hydraulic tortuosity [8–10], while electrical conductivity depends on a single length scale, porosity and electrical tortuosity [3,16], providing surface conduction is neglected [11].

Single value crack damage parameters have been used to model the mechanical properties of rocks [19–23]. These crack damage parameters are derived either from elastic wave measurements [21–23], or from acoustic emission (AE) measurements [19,20]. It is rare, however, that transport properties are used to model the mechanical evolution of a saturated rock sample during deformation [3]. A so-called electrical porosity of a saturated rock can be derived from electrical conductivity measurements [3,24]. This is not a pure measure of effective or connected volumetric porosity because it is also sensitive to the orientation and connectivity of developing and closing cracks. We have hypothesised, therefore, that it should be possible to use electrical porosity as a single value crack damage parameter, which would have the advantage of being sensitive to the same changes in the rock microstructure as the mechanical properties of the deforming rock (crack volume, orientation and connectivity).

The subject of this paper is the measurement of the changes in the crack network, porosity, cementation exponent and electrical tortuosity undergone by a saturated rock when subjected to brittle deformation using electrical conductivity measurements.

2. Samples and experimental procedures

2.1. Sample material

Darley Dale sandstone was used for all experiments. This well indurated granular feldspathic quartz sandstone (75% quartz, 15% feldspar, and 10% muscovite and illite) [25] has grain sizes in the range 0.08–0.8 mm, a medium to high porosity (12–28%), and a high permeability (500–2000 mD) [20,25]. Measurements were performed on right cylinders 40 mm in diameter, and approximately 110 mm in length. Each sample was saturated with initially pure, vacuum-degassed, deionised water [26].

2.2. Electrical conductivity measurements

Complex electrical parameter measurements were made in a two electrode cell (Fig. 1). The electrodes were made from platinum-blacked platinum gauze [16,17,26]. We used a two electrode system for our uniaxial tests [16] and these triaxial deformation experiments because (i) comparative experiments between blacked or un-blacked, two or four electrode systems at laboratory temperatures and pressures showed that the use of two well-blacked platinum electrodes provides data free of electrode polarisation at frequencies greater than 20 Hz, and (ii) two electrodes are much easier to incorporate into a triaxial conductivity cell.

Complex conductivity measurements as a function of frequency, from 20 Hz to 1 MHz, are made using a HP4284A impedance bridge controlled by computer. Software has been written that allows the computer to make lead and vessel capacitance corrections to the data, convert the initial physical measurements into specific measurements, and to log the data. A second correction was subsequently applied to allow for the fact that the geometrical scaling constant employed to convert the physical measurement to the specific measurement changes as the sample is deformed.

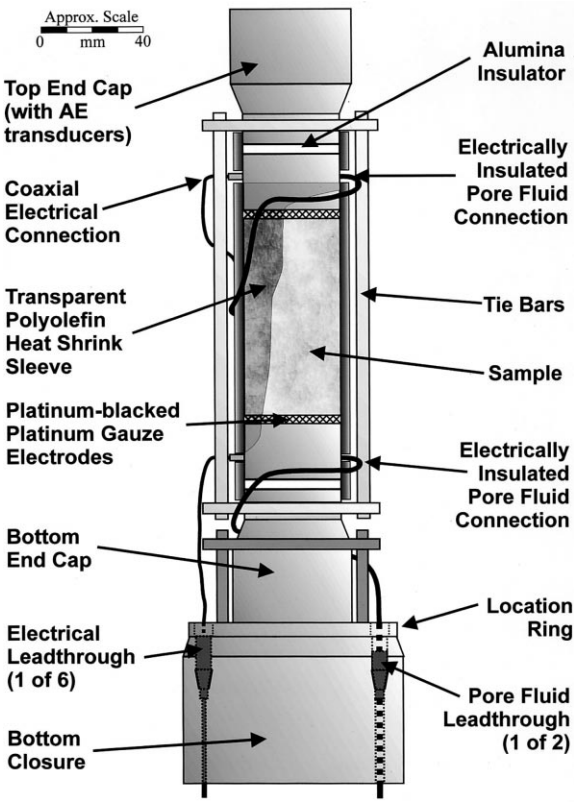

Fig. 1. The two electrode triaxial cell used for triaxial deformation experiments.

All samples were placed in the cell and sleeved with transparent heat shrinkable polyolefin. The cell was placed in a breech loading 400 MPa pressure vessel and 1.5 MN load frame assembly. The whole arrangement is designed in such a way that an experimental charge (Fig. 1) can be constructed upon the bottom end closure, which is slid under the pressure vessel, and the pressure vessel lowered upon it using hydraulic jacks. Both the bottom end closure and the internal bore of the vessel have breech locking threads so that the vessel can be lowered fully over the end closure. A twist of the vessel through 60 degrees then seals the charge inside the vessel, and confining pressure oil can be introduced. The cross-head of the load-frame is then locked, and the load cell brought into contact with a floating balanced ram that penetrates the top closure of the vessel. All subsequent movement of the ram is servo-controlled with a high precision analogue feedback system. Initially a hydrostatic confining pressure of either 25 or 50 MPa was applied in stages, while monitoring changes in the conductivity. Triaxial deformation was then started at a constant strain rate (1.66×10^{-6} s^{-1} for all samples) until failure occurred, while conductivity continued to be monitored.

Both drained and undrained tests were carried out. In the undrained tests, pore fluids were not allowed to drain freely during deformation, and the pore pressure was not monitored. In the drained tests, the pore fluid was allowed to drain freely to atmospheric pressure through electrically insulated pipework, where it was collected in an electrically isolated glass measuring cylinder arranged on an electronic balance in such a way that the mass of expelled/imbibed fluid could be measured. We assumed the fluid density to be constant and equal to that of the fluid used to saturate the rock.

A drained hydrostatic confining pressure test was also carried out up to 250 MPa using the triaxial equipment. This is a simple experiment to carry out because the triaxial pressure vessel and load-frame are equipped with a balanced ram that ensures that the sample is in hydrostatic conditions when no deviatoric stress is applied from the load frame.

2.3. Derivation of microstructural parameters

Various microstructural parameters can be inferred from the electrical and pore fluid measurements made in this work. For the drained hydrostatic and triaxial deformation experiments, the following parameters were derived.

1. The porosity of the sample during hydrostatic pressurisation and during triaxial deformation was calculated using the change in mass of the expelled/imbibed fluids together with knowledge of the initial porosity of the sample. We call this the volumetric porosity henceforth. It is given by:

$$(\phi_{ij})_V = \phi_{oo} + \frac{(M_{oo} - M_{ij})}{V_{ij}\,\rho_f} \quad (1)$$

where, $(\phi_{ij})_V$ is the volumetric porosity at any given hydrostatic pressure i and degree of triaxial deformation j, ϕ_{oo} is the initial porosity of the sample before loading into the pressure vessel, M_{oo} is the initial mass reading on the balance before the experiment, M_{ij} is the mass reading on the balance at a given hydrostatic pressure i and degree of deformation j, ρ_f is the density of the pore fluid, which is assumed to be constant during the experiment (i.e., constant temperature and incompressible pore fluid in the active fluid pressure range), and V_{ij} is the bulk volume of the sample at a given hydrostatic pressure i and degree of deformation j (i.e., corrected for strain).

2. The porosity of the sample during hydrostatic pressurisation and during triaxial deformation was also calculated using a form of Archie's law ($\sigma_r = \sigma_f \phi^m$) together with the fluid conductivity at 1 kHz (σ_f) and the rock conductivity at 1 kHz (σ_r). It is also necessary to assume that the cementation exponent m_{ij} at a raised hydrostatic pressure and degree of deformation remains constant. In this work we have taken it to be equal to that measurable on the sample before the experiment under bench-top conditions (m_{oo}). We call this the electrical porosity henceforth. It is given by:

$$\log (\phi_{ij})_E = \left(\frac{\log \sigma_{r,ij} - \log \sigma_f}{m_{oo}} \right) \quad (2)$$

where, $(\phi_{ij})_E$ is the electrical porosity at any given hydrostatic pressure i and degree of triaxial deformation j, $\sigma_{r,ij}$ is the electrical conductivity of the sample at a given hydrostatic pressure i and degree of deformation j, and σ_f is the electrical conductivity of the pore fluid, which is assumed to be constant during any given experimental run (i.e., temperature is constant and there is no significant dependence of pore fluid conductivity on fluid pressure). The constant value m_{oo} can be calculated using the effective rock conductivity, pore fluid conductivity, and the rock porosity before the experiment at bench-top conditions using Eq. 3 below.

3. The cementation exponent m_{ij} of the sample during hydrostatic pressurisation and during triaxial deformation was calculated using Archie's law, the fluid and rock conductivities at 1 kHz, and the calculated volumetric porosity. It is given by

$$m_{ij} = \left(\frac{\log \sigma_{r,ij} - \log \sigma_f}{\log (\phi_{ij})_V} \right) \quad (3)$$

where all parameters are defined previously, and $(\phi_{ij})_V$ is obtained from Eq. 1.

4. The electrical tortuosity α_{ij} of the sample is a parameter that describes the complexity of the electrical flow through the rock. The reciprocal of tortuosity is the connectivity γ_{ij}. The electrical tortuosity was calculated using

$$\alpha_{ij} = \frac{1}{\gamma_{ij}} = (\phi_{ij})_V^{(1-m_{ij})} \quad (4)$$

where, the cementation exponent m_{ij} is obtained according to Eq. 3, and $(\phi_{ij})_V$ is obtained from Eq. 1.

The assumptions that (i) temperature is constant, (ii) the pore fluid is incompressible, and (iii) the pore fluid conductivity does not change as a function of fluid pressure, are all valid in this work as the temperature was 22 ± 2°C, and the pore fluid pressure in the drained runs (where the assumptions apply) was atmospheric.

For the undrained test, it was not possible to calculate these parameters, as (i) a volumetric porosity was not available, and (ii) the assumption that the conductivity of the pore fluid does not vary with fluid pressure is not valid.

It is important to make the distinction between the electrical porosity and the volumetric porosity because they measure different physical porosities. The volumetric porosity represents the hydraulically connected porosity available for drainage/imbibition. By comparison, the electrical porosity represents the electrically connected porosity and is implicitly weighted to favour cracks that align axially.

3. Results and discussion

3.1. Hydrostatic measurements

Fig. 2 shows the evolution of complex resistivity as a function of frequency and confining pressure for sample TRY3. Both in-phase and out-of-phase components of resistivity increase in approximately the same proportion so the semi-circular curve in the Argand diagram (Fig. 2a) expands but retains its shape. This implies that the application of a hydrostatic confining pressure changes the absolute magnitude of the complex resistivity of the saturated rock sample, but does not affect significantly its frequency dependence. For frequencies less than approximately 10 kHz the response of the in-phase resistivity is flat (Fig. 2b), and the out-of-phase resistivity has very low values (Fig. 2c), indicating that electrode polarisation is negligible and conduction through the rock is almost ohmic. At higher frequencies Fig. 2c clearly shows the electrical dispersion that has been related to non-linear behaviour in the processes of surface conduction [11,15–17]. The out-of-phase dispersion peak occurs at about 600 kHz, and represents non-linearity in surface conduction at periods around 1.67 μs, which is relatively insensitive to changes in applied hydrostatic pressure.

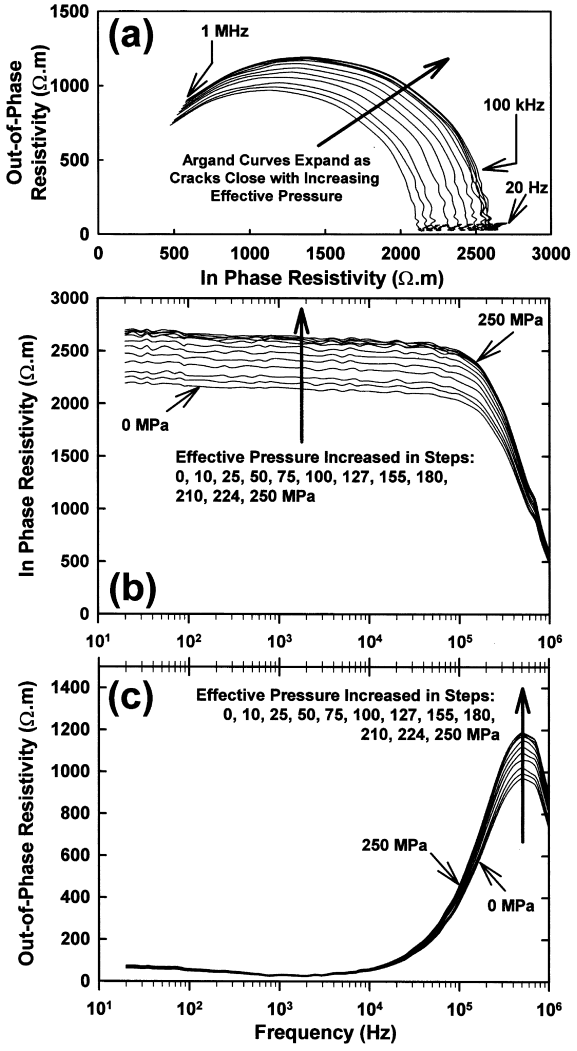

Fig. 2. Complex resistivity as a function of frequency and effective pressure during hydrostatic pressurisation of sample TRY3 in fully drained conditions. (a) Argand resistivity diagram. (b) In-phase electrical resistivity. (c) Out-of-phase electrical resistivity.

The proportionality between the in-phase and out-of-phase components of electrical resistivity can be discerned most easily by taking one frequency such as 1 kHz, as shown in Fig. 3a. The increase in both the in-phase and out-of-phase electrical resistivity per unit increase in confining pressure becomes less as confining pressure increases. This can be attributed to two processes: (i) Thin cracks close easily under the influence of low confining pressures, leading to a large change in pore and crack volume for each unit increase of confining pressure. At progressively higher pressures only pores with more equant geometries remain, and they lose their volume much more grudgingly per unit increase in confining pressure. (ii) The change in electrical conductivity due to loss of a unit volume of a thin crack is much greater than that due to the loss of the same volume of a pore because the thin crack is likely to contribute more to the connectivity of the pore and crack network.

As this is a drained experiment, we can derive various micro-structural parameters from the electrical data using Archie's law [10], as discussed in Section 2.3, above. Fig. 3b shows the volumetric porosity calculated using Eq. 1 and the cementation exponent calculated using Eq. 3. It is clear that the cementation exponent varies by a small

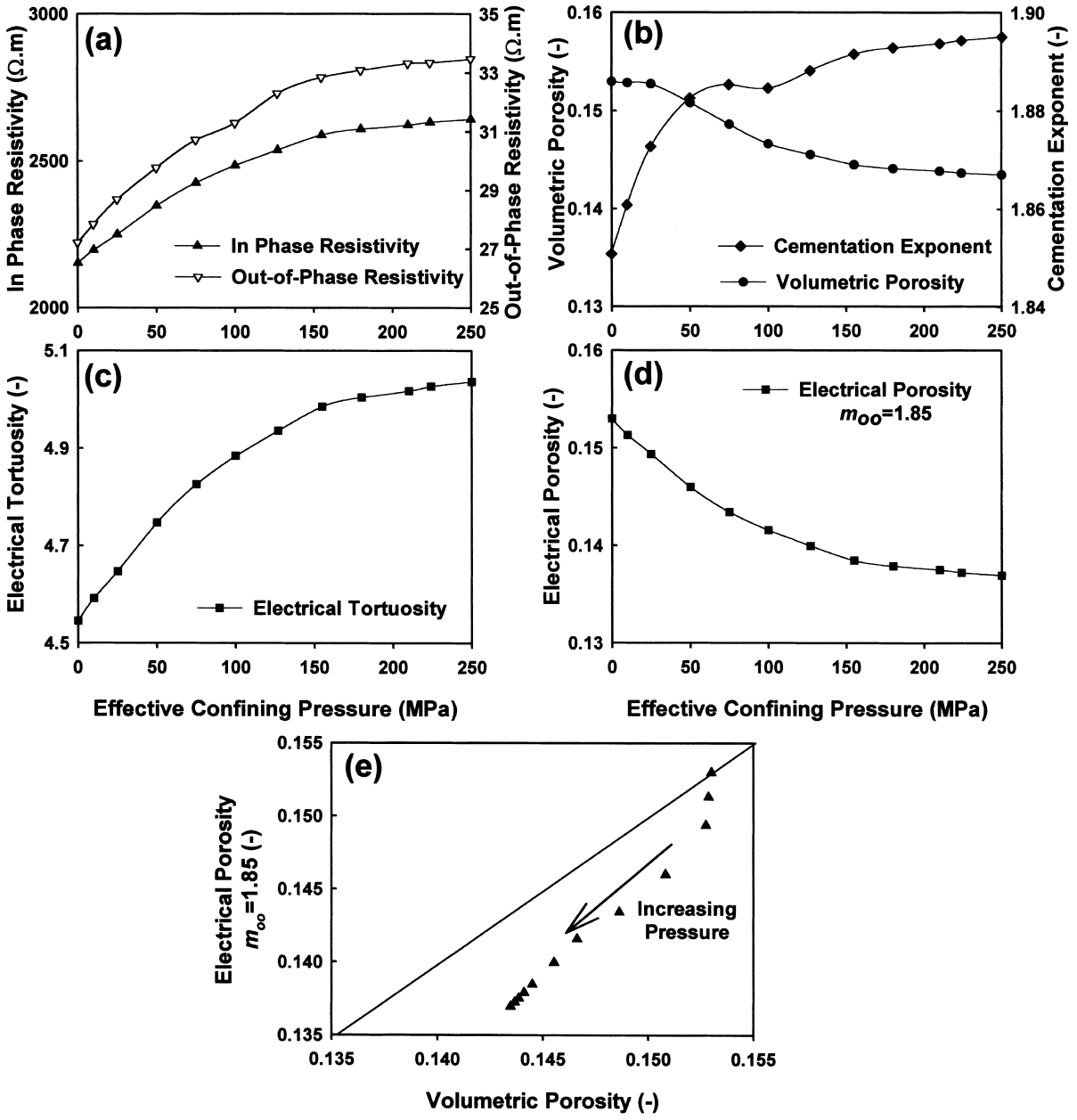

Fig. 3. The electrical and microstructural evolution of sample TRY3 in drained conditions when subjected to hydrostatic pressure. (a) Complex resistivity at 1 kHz. (b) Volumetric porosity and cementation exponent. (c) Electrical tortuosity. (d) Electrical porosity. (e) Crossplot of electrical porosity versus volumetric porosity.

but significant amount during hydrostatic pressurisation, increasing in value as a result of the progressive loss of thin cracks within the rock sample. Fig. 3c shows the electrical tortuosity calculated using Eq. 4. The steady increase in electrical tortuosity is also the result of the progressive closure of thin cracks, which reduces the overall crack connectivity.

The electrical porosity can only be calculated from the raw data using Eq. 2 by assuming a cementation exponent value. The most reasonable experimental cementation exponent to take is the one that can be calculated using Eq. 3 from electrical and porosity measurements on the sample before the experiment has begun. If this is done for TRY3 ($m_{oo} = 1.85$), the derived electrical porosity has a very similar shape to the volumetric porosity (cf., Fig. 3b,d). The electrical porosity has been cross-plotted against the volumetric porosity in Fig. 3e, which shows that the porosities for zero effective confining pressure lie on the 1:1 line. This is because the electrical porosity is calculated using the cementation exponent derived from data taken at zero effective confining pressure, which incorporates the initial volumetric porosity of the sample. The cross-plot trends away from the 1:1 line as pressure is increased due to changes in m_{ij}, but only by a small amount ($\Delta\phi_{ij} = (\phi_{ij})_V - (\phi_{ij})_E < 0.015$, i.e., $\sim 10\%$). We infer from this that, in the absence of an ability to obtain a volumetric porosity (e.g., for undrained samples) the electrical porosity is a reasonable alternative method of deriving the rock porosity during hydrostatic pressurisation. Since it is expected that the cementation exponent m_{ij} will increase slightly during pressurisation, the electrical porosity derived in this way will slightly underestimate the volumetric porosity of the rock.

Each of the triaxial deformation experiments described below were preceded by increasing the confining pressure in stages until the confining pressure at which the deformation was to be carried out was attained. In each case the full electrical parameter set was obtained, resulting in data very similar to Figs. 2 and 3, but up to lower ultimate confining pressures.

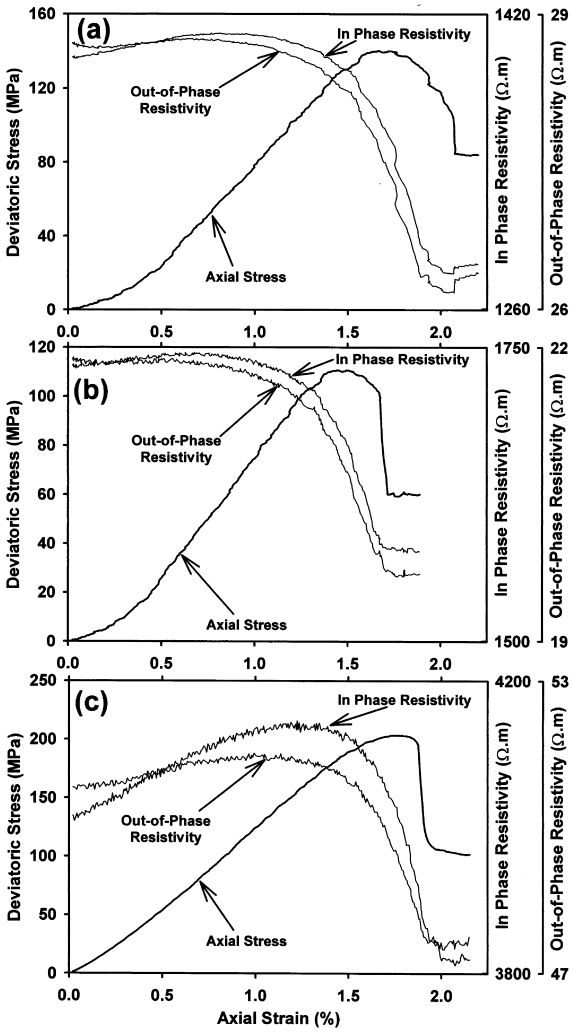

Fig. 4. Complex resistivity at 1 kHz and applied axial stress as a function of axial strain during triaxial deformation for samples of water-saturated Darley Dale sandstone. (a) TRY1 with confining pressure, $P_c = 50$ MPa, undrained, (b) TRY2 with $P_c = 25$ MPa, undrained, (c) TRY4 with $P_c = 50$ MPa, drained.

Table 1
Test information

Sample	Regime	Confining pressure (MPa)	Peak axial stress (MPa)	Axial strain at peak stress (%)	Axial stress at failure (MPa)	Axial strain at failure (%)
TRY1	Triaxial, undrained	50	141.7	1.74	103.2	2.08
TRY2	Triaxial, undrained	25	111.8	1.51	95.6	1.68
TRY3	Hydrostatic	0–355	–	–	–	–
TRY4	Triaxial, drained	50	203.5	1.73	185.3	1.89

3.2. Triaxial deformation measurements

Fig. 4 shows the variation of the complex resistivity at 1 kHz and stress–strain curves for three samples of Darley Dale sandstone in both drained and undrained regimes (Table 1). All samples failed along a single well defined diagonal plane. Comparison of the stress–strain curves clearly shows a well developed strain-softening phase in both of the undrained samples (Fig. 4a,b) that is missing in the drained sample (Fig. 4c). The stiffening effect of the increased confining pressure in TRY1 (Fig. 4a) compared with TRY2 (Fig. 4b) is also clear. The in-phase and out-of-phase resistivity of the two undrained samples are very similar (Fig. 4a,b), but differ markedly from the drained sample (Fig. 4c), which undergoes a greater increase in resistivity. We attribute this to the effect of fluid propping in the undrained samples. In the undrained samples fluid cannot flow out of the cracks and must be compressed in order for the crack to close. By comparison, the fluid occupying cracks in the drained samples are freely expelled when pressure is applied, leading to greater closure, and hence greater increases in the electrical resistivity.

The variation of the complex electrical behaviour at 1 kHz during deformation has the following generic behaviour. In the low axial strain region the primary process operating in the rock is compaction of pores and cracks. Pores and cracks that are most sensitive to closure are (i) thin, and (ii) have orientations perpendicular to the direction of principal stress. The relatively low levels of confining pressure used in these tests result in the direction of principal stress being almost axial for the majority of the deformation. The dominating process at low strains is hence the closure of cracks perpendicular to the direction of this subaxial principal stress. Closure of these cracks has little effect on the saturated rock electrical conductivity because they are perpendicular to the direction of current flow, and their loss provides only a small increase in the tortuosity of the current flow paths. The resulting effect is a small increase in the saturated rock electrical resistivity as cracks perpendicular to the direction of current flow close.

New cracks begin to grow at some value of axial strain in the low strain region. These cracks are aligned in a direction preferentially parallel to the direction of principal stress, and have a large effect on the rock conductivity for two reasons. First, because, at such low values of confining pressure, they are formed roughly in the same direction as the current flow, and second, because their small angle to the axis makes it more likely for cracks to inter-link, increasing the electrical connectivity. The peak in the resistivity curve represents the strain at which the effect on rock resistivity due to crack closure is exactly equaled by the effect of new crack formation. It is interesting to note that the peak occurs well inside the quasi-elastic region of the stress–strain curve, demonstrating that it is naïve to think of the linear portion of the stress-strain curve as representing elastic behaviour. Rather it is the outcome of two competing mechanisms; (i) the closure of a crack population aligned perpendicularly to the axis of deformation, and (ii) the growth and propagation of a population of cracks aligned parallel to the axis of the deforming sample.

For greater axial strains, the effect of new cracks upon the electrical properties of the saturated rocks begins to dominate. This is due to three related contemporaneous processes. First, the tendency for the resistivity to increase due to closure and loss of cracks oriented perpendicular to the sample axis is becoming less as more and more of these cracks cease to be electrically patent. Second, the tendency for the resistivity to decrease due to the formation and dilatancy of cracks parallel to the sample axis is growing. Third, the electrical effect of the loss of a unit volume of crack porosity oriented perpendicular to the sample axis is much less than the effect of the formation of a unit volume of crack porosity parallel to the sample axis, because this is the direction in which gross current flow is occurring within the rock.

At first, the decrease in electrical resistivity is gradual, defining a broad peak in the electrical resistivity. Soon, however, the resistivity decreases sharply due to the combined effect of cracks growing in the same general direction as the current flow, and an ever increasing connectivity as

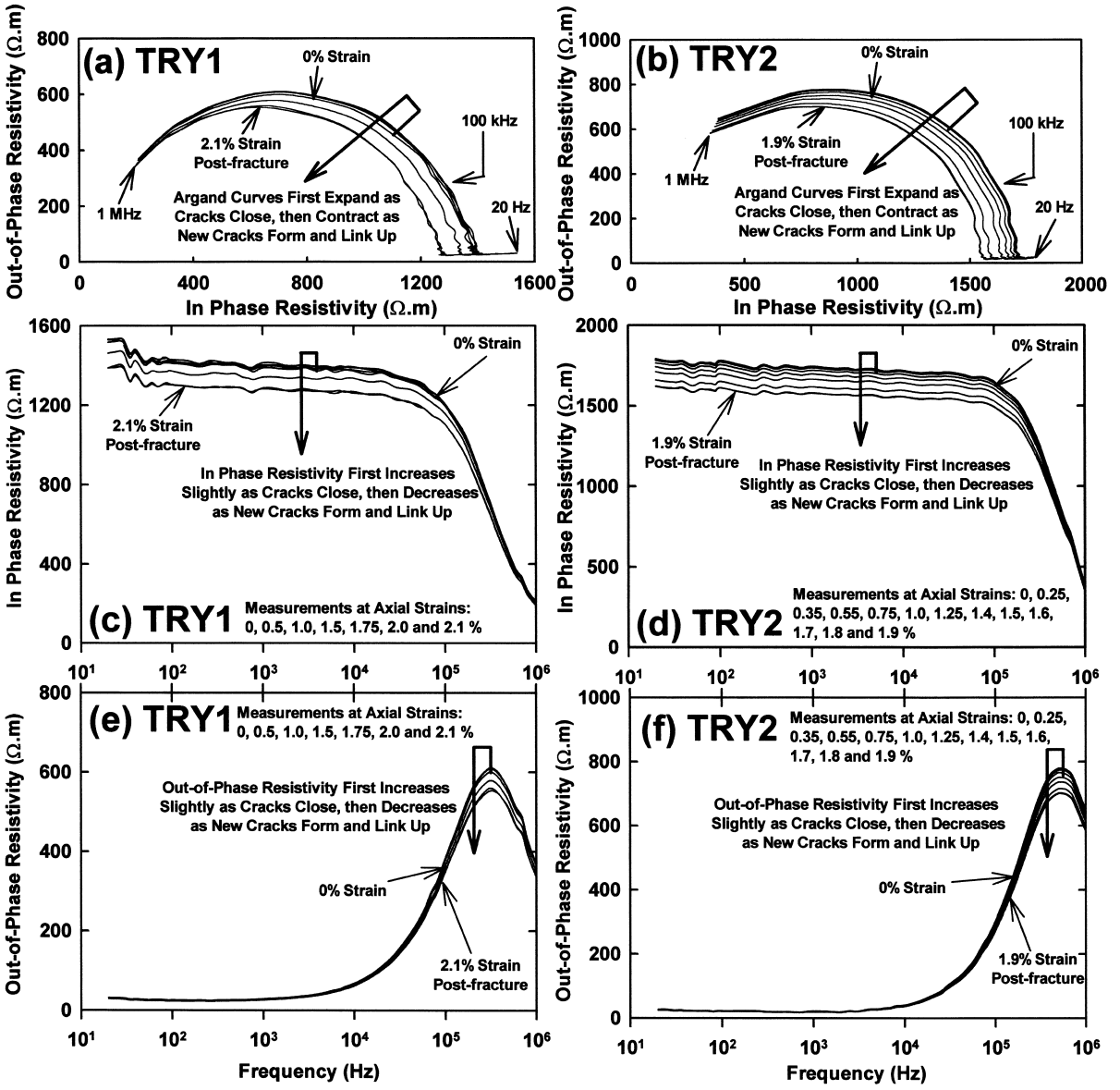

Fig. 5. Complex resistivity as a function of frequency and axial strain during triaxial deformation for samples of water saturated Darley Dale sandstone TRY1 (a,c,e) and TRY2 (b,d,f) in undrained conditions. (a,b) Argand resistivity diagrams. (c,d) In-phase electrical resistivities. (e,f) Out-of-phase electrical resistivities.

cracks inter-link. As axial strain increases further, cracks continue to form and propagate, also leading to a decrease in the stress increment needed to cause axial deformation at a given rate. Eventually crack linking becomes commonplace, dramatically reducing the electrical tortuosity of current flow, and hence reducing resistivity, which continues until failure.

Dynamic rock failure occurs by fracture localisation when sufficient cracks coalesce along a plane intersecting the sample. (In our experiments failures took the classic form of one diagonal

fracture.) Finally, at failure the stress drops to a lower level representing that needed to cause deformation by frictional shearing along the fractures. There is an apparent discontinuity in the electrical resistivity at this point, which results from the failure of the geometric constant when the sample can no longer be considered cylindrical. It is important to note that there is no large decrease in resistivity at failure. This might have been expected, and explained as a result of the formation of one or a few major fluid saturated fractures with large conductivities. Indeed we expect this to be the case for experiments on low porosity saturated crystalline rock samples. It does not occur here because the conduction through the pore structure of the rock (between developing major cracks) remains high throughout the deformation due to the highly porous nature of Darley Dale sandstone.

The frequency dependence of the electrical properties of samples TRY1 and TRY2 is shown in Fig. 5. The conduction in the rock is almost ohmic from 20 Hz up to approximately 20 kHz in both cases, evidenced by the approximately constant in-phase resistivity and the low levels of the out-of-phase resistivity. However the small non-zero gradient of the in-phase resistivity, and the non-zero out-of-phase resistivity in the frequency range indicates that some dispersion is present, which results from the natural electrical tortuosity of the pore and crack network. At frequencies greater than 20 kHz there is a pronounced dispersion centering on 300 kHz and 500 kHz for TRY1 and TRY2, respectively, which is associated with charge transfer processes operating at characteristic timescales of 3.3 and 2.0 μs, respectively.

Both the in-phase and the out-of-phase resistivity change in approximately the same proportion during deformation across the whole frequency range. At low strains both the in-phase and the out-of-phase resistivity undergo small increases associated with the closure of cracks perpendicular to the deformation axis. At large strains, when new crack formation is the dominant process within the rock, both the in-phase and the out-of-phase resistivity decrease strongly until failure, whereupon they remain approximately constant.

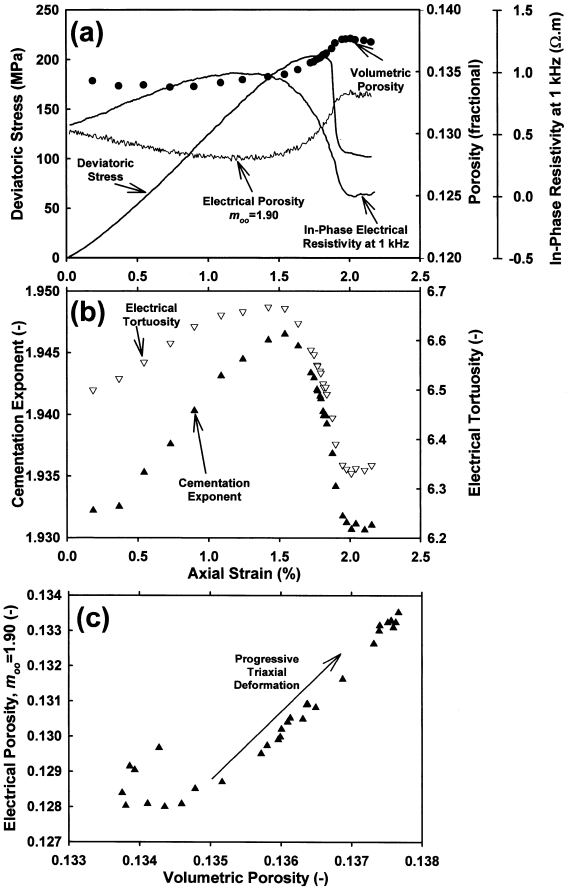

Fig. 6. The microstructural evolution of sample TRY4 in drained conditions when subjected to triaxial deformation. (a) In-phase electrical resistivity, electrical porosity, volumetric porosity and applied axial stress as a function of axial strain. (b) Cementation exponent and electrical tortuosity as a function of axial strain. (c) Crossplot of electrical porosity versus volumetric porosity.

This is the same behaviour as for the particular case at 1 kHz, but extended across the whole frequency range, and implies that triaxial deformation does not affect significantly the frequency dependence of the complex rock conductivity.

3.3. Porosity, cementation exponent and electrical tortuosity

Both the volumetric and electrical porosities of sample TRY4 were obtained during deformation.

Fig. 6a shows the variation in the volumetric porosity (calculated using Eq. 1) and the electrical porosity of sample TRY4 as the deformation progressed. The calculation of the electrical porosity used a value of $m_{oo} = 1.90$, which was the cementation exponent calculated from Eq. 3 using electrical and porosity measurements made at benchtop conditions just prior to the experimental run. At low strains the porosities decrease as cracks perpendicular to the axis are closed. At higher strains the porosities increase due to the formation of new cracks and the propagation of existing cracks oriented parallel to the axis. After failure there is no macroscopic change in the porosity of the sample using either method.

It is clear that the two porosity determinations have a very similar shape (Fig. 6a). The electrical porosity underestimates the volumetric porosity by a small amount ($\Delta\phi_{ij} = (\phi_{ij})_V - (\phi_{ij})_E < 0.006$, i.e., $\sim 4\%$), which arises from the variation in the cementation exponent during the initial application of the 50 MPa confining pressure. The electrical and volumetric porosities have been cross-plotted in Fig. 6c, which shows a hooked line, the linear portion of which has an adjusted coefficient of determination $R^2_a = 0.982$ and a gradient of 1.83. The non-unity gradient is the result of using m_{oo} to represent m_{ij} throughout the deformation, but may also arise partly from differences in the electrical connectivity and the hydraulic (drainage) connectivity of the sample. However, the small differences between the electrical porosity and its volumetric counterpart, combined with the clear correlation, suggests that electrical porosity is a good approximation to the volumetric porosity if the volumetric porosity cannot be calculated directly.

The value of the cementation exponent was also calculated using Eq. 3 during the deformation of sample TRY4 (Fig. 6b). When the sample was subjected to low axial stresses, the cementation exponent increased. This is consistent with our previous interpretations, and represents the continuing closure of thin cracks aligned perpendicular to the direction of principal stress. The increase in the value of the cementation exponent continues while the electrical resistivity increases, as expected, and reaches a peak at a value of axial strain between that at which the resistivity reaches its peak value and that at which the peak stress occurs. This is the value of axial strain where the change in the cementation exponent due to closure of cracks arranged perpendicular to the direction of stress and conductivity measurement is the same as that due to the formation of new cracks oriented sub-parallel to the axis of deformation and conductivity measurement. Subsequently, the cementation exponent decreases due to the proliferation of new cracks forming and propagating sub-parallel to the axis of deformation, until the value becomes constant after failure when the rock matrix is subjected to a lower value of axial deviatoric stress, which is controlled by the load that is necessary to cause the fault plane to shear at the constant set strain rate.

Fig. 6b shows the variation of electrical tortuosity, calculated using Eq. 4, as a function of axial strain for sample TRY4. The electrical tortuosity rises at low axial strains due to the compactive loss of paths for electrical transport. As axial strain increases, new cracks begin to form, and their effect is to reduce the overall electrical tortuosity of the network. The electrical tortuosity curve reaches a maximum when the effect of the compacting cracks and the growing cracks on electrical tortuosity balance each other. Subsequently the electrical tortuosity decreases substantially as the new cracking becomes dominant, and crack inter-linking occurs just prior to failure, as previously noted. The most substantial decline in

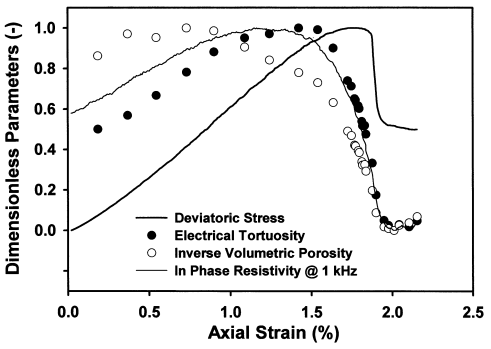

Fig. 7. Comparison of how major micro-structural parameters change during triaxial deformation for sample TRY4 in drained conditions. All data normalised to lie between 0 and 1.

electrical tortuosity occurs between peak stress and failure. After failure the electrical tortuosity remains constant.

We have taken a range of parameters that were either measured during deformation of sample TRY4 or calculated from those measurements. These parameters have been normalised between their lowest and highest values to aid comparison between them (Fig. 7). Referring to Fig. 7; the first curve to peak is that of the inverse volumetric porosity, at 0.75% axial strain. Thus below 0.75% strain net loss of volumetric porosity occurs in the sample; and subsequently there is a net gain in volumetric porosity due to the dominance of new crack formation over compaction. The electrical resistivity, however, continues to rise after 0.75% axial strain is reached because it depends both on the inverse porosity and the electrical tortuosity of the rock sample, and the continued increasing electrical tortuosity exerts stronger control over the electrical resistivity in this region. The electrical resistivity peaks (1.2% axial strain) before the electrical tortuosity (1.5% axial strain). The position of the peak electrical resistivity is defined by both the inverse porosity (representing the way that the rock resistivity depends upon the volume of the conducting fluid within the rock), and the electrical tortuosity (representing the way that conducting fluid volume is geometrically arranged within the rock). It is instructive to compare the behaviours of the inverse porosity and the electrical tortuosity curves. It is plain from the inverse porosity curve that new crack formation begins before 0.75% axial strain, and begins to have a dominant effect on the electrical resistivity at 1.2% axial strain, but only begins to control the electrical tortuosity at 1.5% axial strain. Thus between the axial strains of 0.75% and 1.5% new crack growth occurs, but in such a way that it does not increase the connectivity of the pore and crack network greatly. We infer from this that the progressive closure of cracks perpendicular to the axis limits the extent to which newly formed and propagating cracks in the axial direction can inter-connect. This delays the occurrence of gross inter-linkage of cracks until late in the deformation, when the development of new cracks parallel to the axis has become sufficiently large to inter-connect without the aid of bridging cracks perpendicular to them. Thus, the development of a crack matrix with a low electrical tortuosity (i.e., high connectivity) is confined to axial strains just prior to failure.

4. Conclusions

Measurement of the complex electrical parameters of saturated rocks provides information concerning the closure, formation and growth of cracks during triaxial deformation. Electrical parameters are particularly sensitive to the orientation of the cracks that are closing, opening or propagating. The major conclusions of this paper are as follows.

1. The onset of new crack formation occurs well inside the quasi-linear part of the stress–strain curve.
2. The quasi-linear portion of the stress–strain curve is the result of competition between closure of one population of cracks oriented perpendicular to the axis, and growth of new and propagation of existing cracks parallel to the axis, rather than true elastic behaviour.
3. The relative importance of crack closure and dilatation during deformation, and between crack populations controls the observed volumetric porosity, electrical porosity, cementation exponent, electrical tortuosity, and the resulting electrical data over a wide range of frequencies.
4. The development of large scale connectivity (indicated by large drops in electrical tortuosity) is observed to be confined to just prior to failure, because of the loss of cracks perpendicular to the axis of current flow and deformation.
5. The frequency dependence of the complex electrical conductivity of these moderate porosity, high permeability sedimentary rock samples was found to be not affected significantly by the process of hydrostatic pressurisation and triaxial deformation.

Acknowledgements

The authors would like to thank S.A. Boon, P.R. Sammonds and S.A.F. Murrell for their contributions to the original design and construction of the mechanical apparatus used in this work. Many thanks to J. Mack, S. Raab and an anonymous reviewer for constructive comments.*[AC]*

References

[1] A.M. Wulff, S. Raab, E. Huenges, Alteration of seismic wave properties and fluid permeability in sandstones due to microfracturing, Phys. Chem. Earth 25 (2000) 141–147.
[2] E. Eberhardt, D. Stead, B. Stimpson, Quantifying progressive pre-peak brittle fracture damage in rock during uniaxial compression, Int. J. Rock Mech. Min. Sci. Geomech. Abstr. 36 (1999) 361–380.
[3] P.W.J. Glover, J.B. Gómez, P.G. Meredith, S.A. Boon, P.R. Sammonds, S.A.F. Murrell, Modelling the stress-strain behaviour of saturated rocks undergoing triaxial deformation using complex electrical conductivity measurements, Surv. Geophys. 17 (1996) 307–330.
[4] C. David, B. Menendez, M. Darot, Influence of stress-induced and thermal cracking on physical properties and microstructure of La Peyratte granite, Int. J. Rock Mech. Min. Sci. Geomech. Abstr. 36 (1999) 433–448.
[5] E. Huenges, G. Zimmermann, Rock permeability, fluid pressure at the KTB – implications from laboratory – and drill hole – measurements, Oil Gas Sci. Tech. Rev. Inst. Fr. Pet. 54 (1999) 689–694.
[6] Y. Guéguen, P. Gavrilenko, M. LeRavalec, Scales of rock permeability, Surv. Geophys. 17 (1996) 245–263.
[7] A.E. Scheidegger, The Physics of Flow through Porous Media, University of Toronto Press, Toronto, 1974, 353 pp.
[8] Y. Bernabé, The transport properties of networks of cracks and pores, J. Geophys. Res. 100 (1995) 4231–4241.
[9] Y. Bernabé, A. Revil, Pore scale heterogeneity, energy dissipation and the transport properties of rocks, Geophys. Res. Lett. 22 (1995) 1529–1530.
[10] Y. Guéguen, V. Palciauskas, Introduction to the Physics of Rocks, Princeton University Press, Princeton, NJ, 1994, 294 pp.
[11] A. Revil, P.W.J. Glover, Theory of ionic electrical conduction in porous media, Rev. Phys. B 55 (1997) 1757–1773.
[12] G. Nover, S. Heikamp, H.J. Meurer, D. Freund, In situ electrical conductivity and permeability of mid-crustal rocks from the KTB drilling: Consequences for high conductive layers in the earth crust, Surv. Geophys. 19 (1998) 73–85.
[13] T.L. Chelidze, Y. Guéguen, Electrical spectroscopy of porous rocks: a review – I. Theoretical models, Geophys. J. Int. 137 (1999) 1–15.
[14] T.L. Chelidze, Y. Guéguen, C. Ruffet, Electrical spectroscopy of porous rocks: a review – II. Experimental results and interpretation, Geophys. J. Int. 137 (1999) 16–34.
[15] D.A. Lockner, J.D. Byerlee, Complex resistivity measurements of confined rock, J. Geophys. Res. 90 (1985) 7837–7847.
[16] P.W.J. Glover, P.G. Meredith, P.R. Sammonds, S.A.F. Murrell, Measurements of complex electrical conductivity and fluid permeability in porous rocks at raised confining pressures, in: Rock Mechanics in Petroleum Engineering, Proceedings of EUROCK '94, SPE/ISRM International Meeting, Delft, The Netherlands, Balkema, Amsterdam (1994) 29–36.
[17] P.W.J. Glover, J.B. Gómez, P.G. Meredith, K. Hayashi, P.R. Sammonds, S.A.F. Murrell, Damage of saturated rocks undergoing triaxial deformation using complex electrical conductivity measurements experimental results, Phys. Chem. Earth 22 (1997) 57–61.
[18] C. Ruffet, Y. Guéguen, M. Darot, Complex conductivity measurements and fractal nature of porosity, Geophysics 56 (1991) 758–768.
[19] S.J.D. Cox, P.G. Meredith, Microcrack formation and material softening in rock measured by monitoring acoustic emissions, Int. J. Rock Mech. Min. Sci. Geomech. Abstr. 30 (1993) 11–24.
[20] P.R. Sammonds, P.G. Meredith, S.A.F. Murrell, I.G. Main, Modelling the damage evolution in rock containing a pore fluid by acoustic emission, in: Rock Mechanics in Petroleum Engineering, Proceedings of EUROCK '94, SPE/ISRM International Meeting, Delft, The Netherlands, Balkema, Amsterdam (1994) 897–904.
[21] M.R. Ayling, P.G. Meredith, S.A.F. Murrell, Microcracking during triaxial deformation of porous rocks monitored by changes in rock physical-properties 1 Elastic-wave propagation measurements on dry rocks, Tectonophysics 245 (1995) 205–221.
[22] R.J. O'Connell, B. Budiansky, Seismic velocities in dry and saturated cracked solids, J. Geophys. Res. 79 (1974) 5412–5426.
[23] N. Soga, H. Mitzutani, H. Spetzler, R.J. Martin, The effect of dilatancy on velocity anisotropy in Westerly granite, J. Geophys. Res. 83 (1978) 4451–4456.
[24] J.B. Gómez, P.W.J. Glover, P.G. Meredith, Damage of saturated rocks undergoing triaxial deformation using complex electrical conductivity measurements: mechanical modelling, Phys. Chem. Earth 22 (1997) 63–68.
[25] I.A.H. Ismail, S.A.F. Murrell, Dilatancy and the strength of rocks containing pore water under undrained conditions, Geophys. J. R. Astron. Soc. 44 (1976) 107–134.
[26] P.W.J. Glover, P.G. Meredith, P.R. Sammonds, S.A.F. Murrell, Ionic surface electrical conductivity in sandstone, J. Geophys. Res. 99 (1994) 21635–21650.